KSOE

Journal of Ocean Engineering and Technology 38(5), 245-256, October, 2024
https://doi.org/10.26748/KSOE.2024.053

pISSN 1225-0767
eISSN 2287-6715

Original Research Article

Optimization of BOG Reliquefaction Process of Carbon Dioxide Considering Nitrogen Content

Ijun Jeong[1] and Youngsub Lim[2]

[1]*Graduate Student, Department of Naval Architecture and Ocean Engineering, Seoul National University, Korea*
[2]*Professor, Department of Naval Architecture and Ocean Engineering, Seoul National University, Seoul, Korea*

KEYWORDS: CO_2 carrier, CO_2 BOG reliquefaction, Process optimization, Single mixed refrigerant, Process design

ABSTRACT: *As the importance of carbon capture and storage (CCS) technology increases for greenhouse gas reduction, CO_2 transportation technology is also becoming crucial. Efficiently handling boil-off gas (BOG) generated during voyages is particularly important. This paper proposes a process incorporating two-stage separation and mixed refrigerants to reliquefy CO_2 BOG containing nitrogen efficiently. This process was optimized based on specific power consumption (SPC) criteria and compared with the conventional single-stage separation using an ammonia refrigerant. The two-stage separation allows the removal of non-condensable gases, such as nitrogen, before expansion, and the use of mixed refrigerants enables more efficient heat exchange than ammonia refrigerants, improving the reliquefaction rate. As a result, the proposed process reduced SPC by up to 8.8 % with a nitrogen content of 5 mol% and up to 74.7 % with a nitrogen content of 15 mol%. In addition, the proposed process achieved a reliquefaction rate of over 74.2 % across all nitrogen content ranges of 5–15 mol%.*

Nomenclature

Abbreviation	
CCS	Carbon capture and storage
BOG	Boil-off gas
LNG	Liquefied natural gas
PT diagram	Pressure temperature diagram
EOS	Equation of state
CPA	Cubic plus association
SPC	Specific power consumption
LCO_2	Liquefied CO_2
BOR	Boil-off rate
PSO	Particle swarm optimization
JT	Joule Thomson
Symbols	
W_{total}	Total energy consumption (kW)
$\dot{m}$	Mass flow rate (t/h)
r	Return LCO_2 fraction
V	Volume (m^3)
v	Molar volume (m^3/kgmole)
x	Vapor mole fraction
PR_{Comp}	Pressure ratio of the compressor
P	Pressure (bar)
T	Temperature (℃)
C2	Ethane
C3	Propane
nC4	Normal butane
iC4	Iso butane

1. Introduction

With the adoption of the Paris Agreement in 2015, which aimed to limit the increase in average global temperature to below 2 ℃ compared to pre-industrial levels and restrict it to no more than 1.5 ℃, reducing greenhouse gas emissions has become a significant global issue in response to rapid climate change caused by global warming. IRENA (2022) mentions carbon capture and storage (CCS) as one of the key technologies for achieving greenhouse gas emission reduction targets and expects it to account for approximately 20% of greenhouse gas reductions by 2050. Therefore, the need for research to effectively capture, transport, and store carbon is increasing.

Pipelines and liquefied CO_2 carriers can be considered for transporting captured CO_2 to storage sites efficiently. In particular,

Received 17 May 2024, revised 17 July 2024, accepted 29 August 2024
Corresponding author Youngsub Lim: +82-2-880-7325, s98thesb@snu.ac.kr

shipping was reported to be more economical for long-distance transport. In the case of shipping, liquefaction reduces the volume of CO_2, allowing more mass of CO_2 to be transported per unit volume. Decarre et al. (2010) reported that transport by ship is economically more advantageous than pipeline transport when the distance to the storage site exceeds 1,000 km.

The problem of boil-off gas (BOG) can occur while transporting liquefied CO_2 by ship because liquefied CO_2 must be stored at temperatures lower than room temperature. Although onboard storage tanks are insulated, they cannot block heat ingress completely. Therefore, liquefied CO_2 evaporates due to external heat influx, and the resulting BOG increases the pressure in the storage tank, potentially causing safety accidents. If the generated BOG is vented to the atmosphere to prevent overpressure, it results in cargo loss and greenhouse gas emissions. A BOG reliquefaction process to prevent this can be crucial in minimizing greenhouse gas emissions and ensuring the safety of the CCS supply chain.

Existing studies have mainly focused on the liquefaction process of captured CO_2. Alabdulkarem et al. (2012) proposed a new liquefaction system applying various refrigerants to improve the efficiency of the CO_2 liquefaction process for CCS. Lee et al. (2015) modeled the process for liquefying captured CO_2 and studied changes in process efficiency according to seawater temperature variations Seo et al. (2015) used ammonia, propane, and R-134a as refrigerants in the CO_2 liquefaction process. They reported that ammonia showed the best efficiency. Seo et al. (2016) modeled the Linde–Hampson process and a process using external refrigerants to liquefy captured CO_2 within the CCS value chain. They conducted a cost analysis according to liquefaction pressure. Deng et al. (2019) modeled a liquefaction process using ammonia refrigerant and performed economic evaluations of captured CO_2 based on different scenarios. Aliyon et al. (2020) modeled and analyzed energy, exergy, and economic aspects of the Linde–Hampson process, a process using ammonia refrigerant and an absorption refrigeration process for the liquefaction of captured CO_2. Nevertheless, these studies focused only on the CO_2 liquefaction process and did not consider the reliquefaction process of CO_2 BOG occurring during ship transport.

Some studies on CO_2 BOG reliquefaction systems have been conducted but have limitations. Yoo (2017) studied a CO_2 BOG reliquefaction system using LNG cold energy on an LNG-fueled CO_2 carrier. Lee et al. (2017a) proposed a CO_2 BOG reliquefaction process and presented optimal designs considering the seawater temperature and compressor discharge temperature. Lee et al. (2024) modeled a CO_2 BOG reliquefaction system using the Linde–Hampson process, a process using ammonia refrigerant, and a subcooling process, comparing them based on the liquefaction pressure. On the other hand, these studies have the limitation of assuming CO_2 BOG as pure CO_2. In the CO_2 capture process, various impurities can be mixed into the liquid CO_2. According to Jeon et al. (2015), substances with low boiling points as impurities, such as nitrogen, rapidly vaporize within the liquid CO_2 storage tank, making CO_2 BOG a mixture containing more impurities than the liquid form. CO_2 BOG mixed with nitrogen requires lower temperatures for liquefaction; therefore, an effective reliquefaction process capable of cooling to lower temperatures than pure CO_2 is needed. This leads to increased energy consumption and costs, making research on efficient reliquefaction methods for impurity-containing CO_2 BOG an important topic in liquefied CO_2 transport.

Some studies examined reliquefying impurity-containing CO_2 BOG, but they had limitations. Chu et al. (2012) reported that BOG generated during the transport of captured CO_2 from thermal power plants contains impurities, such as nitrogen and oxygen, and proposed an ethylene–propane cascade cycle as a reliquefaction process. Lee et al. (2017b) proposed and compared four processes using CO_2 as a refrigerant to reliquefy CO_2 BOG containing 36 mol% nitrogen. Using the cascade cycle increased the process complexity because separate compression trains were required for each refrigerant. Cooling below −65.6 ℃ was necessary to achieve a reliquefaction rate of over 98% for impurity-containing BOG, which poses a risk of dry ice formation. In addition, using CO_2 as a refrigerant required compressing CO_2 to high pressures exceeding 100 bar compared to external refrigerants. To achieve a CO_2 reliquefaction rate of 90%, they proposed a process applying a distillation column to separate nitrogen and CO_2, but this increased energy consumption by approximately 1.5 fold compared to other processes.

The use of mixed refrigerants in the liquefaction of mixtures has also been studied widely. Existing low-temperature liquefaction processes, such as natural gas liquefaction and LNG BOG reliquefaction, use liquefaction processes using mixed refrigerants, reporting higher efficiency compared to single-refrigerant liquefaction processes. Using mixed refrigerants in natural gas liquefaction can increase efficiency compared to nitrogen single-refrigerant cycles or cascade cycles by reducing the temperature difference between hot and cold streams in the heat exchanger (Moein et al., 2015; Zhang et al., 2020). According to Lee et al. (2023), using mixed refrigerants in LNG BOG reliquefaction reduced power consumption by 30% compared to using single nitrogen refrigerants. Xu et al. (2013) reported that the composition of mixed refrigerants plays a significant role in the heat exchange efficiency of the process of natural gas liquefaction. On the other hand, such processes using mixed refrigerants have mainly been applied to natural gas liquefaction, and studies optimizing the composition of mixed refrigerants for impurity-containing CO_2 BOG mixtures are difficult to find.

This paper proposes an optimal process design that enables efficient BOG reliquefaction even under temperature constraints to avoid dry ice formation by incorporating a mixed refrigerant liquefaction process into the reliquefaction of impurity-containing CO_2 BOG mixtures. The CO_2 BOG reliquefaction process using ammonia single refrigerant proposed by Seo et al. (2015) was compared. In the reliquefaction process, mixed refrigerants were applied, and a process incorporating a vapor–liquid separator before expansion was proposed to improve the reliquefaction rate.

2. Background

2.1 Characteristics of Carbon Dioxide (CO_2) BOG

Fig.1 presents a pressure-temperature (PT) diagram generated using the commercial software Multiflash V7.0 for CO_2 containing nitrogen impurities ranging from 0 to 15 mol%. The equation of state (EOS) used to plot the graph was CPA-Infochem, which has been reported to predict the phase behavior of CO_2 mixtures accurately (Tsivintzelis and Kontogeorgis, 2015).

Pure CO_2 can be liquefied and stored at various pressures between its triple point (5.1 bar, −56.6 °C) and critical point (73.8 bar, 31.1 °C). Seo et al. (2016) reported that storage pressures above 25 bar are uneconomical when evaluating the cost-effectiveness at various pressures within the CCS value chain, including CO_2 liquefaction systems, storage tanks, and CO_2 carriers. The most commonly mentioned storage pressures between the triple point and 25 bar are two conditions: pressures near the triple point of CO_2 at 6.5−7.0 bar (Chu et al., 2012; Lu et al., 2023; Yoo, 2017) or at 15 bar (Jackson and Brodal, 2019; Lee et al., 2024).

In addition, the dew point temperature decreases as nitrogen impurities increase, requiring lower temperatures for liquefaction. On the other hand, dry ice can form at low temperatures near the triple point. Therefore, in the design of the liquefaction process, care must be taken to ensure that the operating temperature does not fall below the gas−solid phase transition temperature. Consequently, it is necessary to consider this when designing the reliquefaction process and develop a design that can achieve a low dew point temperature while avoiding the range where dry ice forms.

2.2 Carbon Dioxide Liquefaction Process

Fig. 2 shows the single-refrigerant liquefaction processes commonly used in CO_2 liquefaction. CO_2 is compressed to high pressure through a CO_2 compressor and then cooled to low temperatures via heat exchange with a refrigerant in a heat exchanger (Fig. 2(a)). Subsequently, it undergoes partial liquefaction by expanding to the tank pressure through a Joule−Thomson valve. The gas and liquid are separated in a vapor−liquid separator; the gas returns to the front end of the compressor after heat exchange, and the liquid flows into the CO_2 storage tank. Fig. 2(b) presents a process where low-temperature refrigerant is produced through a refrigeration cycle applying

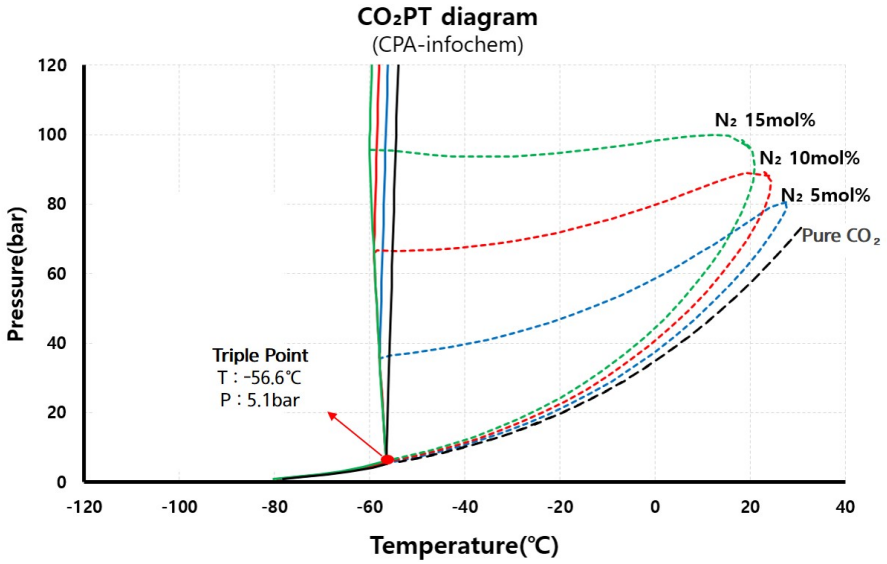

Fig. 1 CO_2 P-T diagram by Multiflash V 7.0

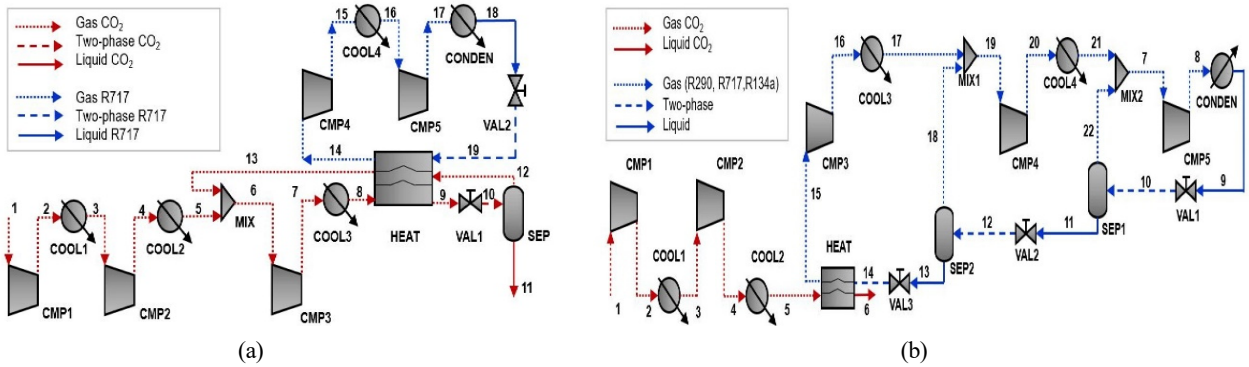

(a) (b)

Fig. 2 CO_2 liquefaction process using (a) precooled Linde−Hampson and (b) multi-stage vapor compression cycle (Chen and Morosuk, 2021)

three-stage expansion, and liquefied CO_2 is produced by heat exchange with CO_2. Although the process becomes more complex than Fig. 2(a) due to multi-stage expansion in the refrigeration cycle, energy consumption can be reduced (Chen and Morosuk, 2021). On the other hand, these conventional reliquefaction processes are designed assuming the liquefaction of pure CO_2. When liquefying CO_2 containing impurities such as nitrogen, a lower liquefaction temperature is required compared to pure CO_2, so it is necessary to design a separate process.

2.3 Efficiency Indices of Carbon Dioxide (CO_2) BOG Reliquefaction Processes

There are various indices to evaluate the performance of CO_2 BOG reliquefaction processes, with Specific Power Consumption (SPC) being widely used (Lee et al., 2017b; Lee et al., 2024). The SPC refers to the total energy consumed to produce one ton (t) of liquefied CO_2 and was calculated as shown in Eq. (1)

$$\text{SPC} = \frac{W_{total}}{\dot{m}_{reliq}} \tag{1}$$

W_{total} is the total power consumption (kW) of the compressors within the reliquefaction system, and $\dot{m}_{reliq}$ is the amount of reliquefied CO_2 (t/h). In this case, the unit of SPC is kWh/t_{CO2}. The lower the total power consumption relative to the amount of liquefied CO_2, i.e., a lower SPC value indicates a better reliquefaction performance.

The CO_2 reliquefaction rate (Return LCO_2 fraction, r) is used to assess the proportion of liquefied CO_2 resulting from the reliquefaction process and was calculated using Eq. (2) (Lee et al., 2017b).

$$r = \frac{\dot{m}_{reliq}}{\dot{m}_{feed}} \tag{2}$$

where $\dot{m}_{feed}$ represents the amount of CO_2 entering the process (t/h). That is, the reliquefaction rate is the ratio of liquefied CO_2 to the amount of CO_2 entering the process. In this study, SPC and the reliquefaction rate were used as indices to evaluate the performance of the reliquefaction process and compare the processes with each other.

2.4 Particle Swarm Optimization (PSO)

PSO is an optimization method developed by Kennedy and Eberhart (1995) that does not require differentiation and can solve non-convex problems. The PSO algorithm starts with randomly initialized particles that update their positions and velocities to find the optimal position. Each particle individually tracks its optimal solution and leverages the discoveries of other particles, allowing the entire swarm to converge quickly on the optimal position. Through this approach, various design variables can be optimized simultaneously, effectively solving nonlinear and multidimensional problems in liquefaction processes (Khan and Lee, 2013). This PSO method has been used in many optimization studies of liquefaction processes (Khan and Lee, 2013; Lee et al., 2024).

3. Process Simulation Conditions

3.1 Carbon Dioxide Storage Conditions

Among the storage pressures for CO_2, the most frequently mentioned are 6.5 bar and 15 bar. Considering the density of liquefied CO_2 in saturated conditions, the density was 1154.6 kg/m³ and 1031.7 kg/m³ at 6.5 bar and 15 bar, respectively. This means that at 6.5 bar, the amount of liquefied CO_2 that can be stored per unit storage volume increased by approximately 12% compared to 15 bar (Jeon et al., 2015). For this reason, the storage pressure of the CO_2 tank was assumed to be 6.5 bar in this paper.

The unit capacity of the CO_2 storage tank applied in this study was set to 100,000 m³ following the assumption of Chu et al. (2012), and it was assumed that the tank is filled up to an initial liquid level of 95% and operated. The boil-off rate (BOR), which is the amount of BOG generated during one day, is typically evaluated at 0.12%–0.2% (Chu et al., 2012; Yoo, 2017). In this study, a BOR of 0.13% was assumed, resulting in a BOG generation amount of 6,000 kg/h. The pressure of the generated BOG was assumed to be the same as the storage pressure, 6.5 bar.

The saturation temperature of CO_2 at 6.5 bar was −50.3 °C. However, in the case of large-scale storage tanks for liquefied cryogenic fluids, heated gas accumulates at the top due to external heat ingress, existing as superheated gas. Therefore, it was assumed that the temperature of the BOG increased to −28.5 °C when entering the reliquefaction facility (Chu et al., 2012).

Table 1 CO_2 BOG and Cargo Tank conditions (Chu et al., 2012)

Item	Unit	Value
Cargo tank pressure	bar	6.5
Cargo capacity	m³	100,000
Cargo density	kg/m³	1154.6
Initial filling ratio	%	95
Boil off rate	%/day	0.13
BOG load	kg/h	6,000
BOG pressure	bar	6.5
BOG temperature	℃	−28.5

3.2 Carbon Dioxide BOG Composition

The CO_2 loaded onto the ship exists as both boil-off gas and liquid CO_2 after loading, and the volumetric ratio of the gas space in the storage tank is called the ullage. The ullage can be estimated based on the volumetric ratio of liquid and gas using Eq. (3).

$$\text{Ullage} = \frac{V_{vap}}{V_{vap+V_{liq}}} = \left[\frac{v_{vap}}{v_{liq}}\frac{x}{(1-x)}\right] \Big/ \left[1+\frac{v_{vap}}{v_{liq}}\frac{x}{(1-x)}\right] \tag{3}$$

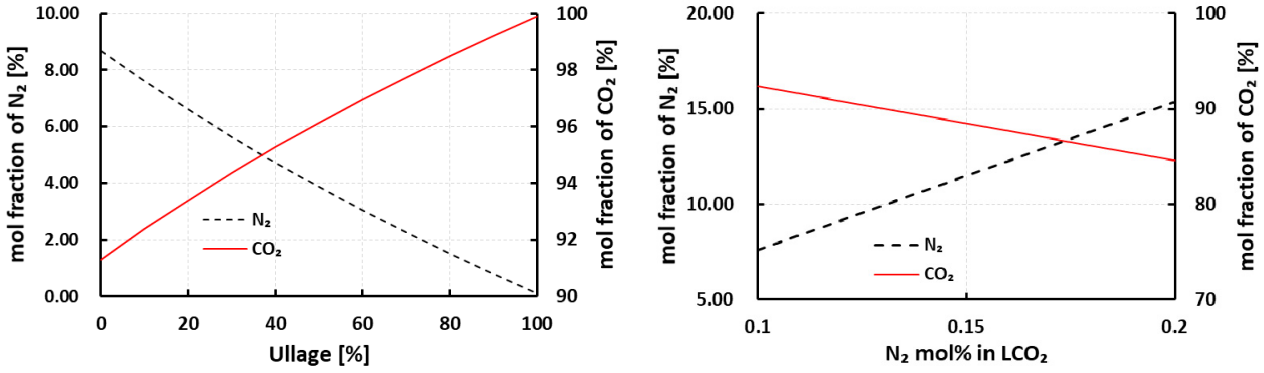

(a) (b)

Fig. 3 Variation of the BOG mole fraction depending on (a) ullage change at 0.1 mol% N_2 and (b) N_2 composition change at ullage 10%

where V_{vap} and V_{liq} represent the volumes occupied by the gas and liquid in the tank, respectively. v_{vap} and v_{liq} denote the molar volumes of the gas and liquid at that time, and x is the vapor mole fraction. This study calculated the vapor mole fraction corresponding to the volumetric ratio of liquid and gas using the commercial software Aspen HYSYS V11, and estimated the gas composition at that time as the BOG composition. When volatile impurities are present in liquefied CO_2, the composition of the boil-off gas at equilibrium changes according to the ullage ratio (Jeon et al., 2015). The total volume of the tank was fixed to 100,000 m³, and a decrease in the value of ullage means that the space occupied by BOG in the tank decreases. As the space occupied by BOG decreases, the mole fraction of nitrogen, which vaporizes more readily than CO_2, increases compared to when the space is larger. Fig. 3(a) shows the change in the mole fraction of nitrogen in CO_2 BOG according to ullage when assuming that liquid CO_2 has a composition of 0.1 mol% nitrogen and 99.9 mol% CO_2, reaching equilibrium at 6.5 bar. The mole fraction of nitrogen increases as the ullage space in the tank decreases, causing the nitrogen mole fraction in the CO_2 BOG to vary from 0.1% to 8.7 mol%. The nitrogen mole fraction in CO_2 BOG was estimated to range from 7.6% to 15.4 mol% when the nitrogen concentration in liquid CO_2 was changed from 0.1 mol% to 0.2 mol% at 6.5 bar and 10% ullage (Fig. 3(b)). In other words, even if only a small amount of nitrogen was included in liquid CO_2, a relatively large amount of nitrogen impurities may exist in the CO_2 BOG, which becomes an important consideration in the reliquefaction cycle. This study compared the optimized performance results of each reliquefaction cycle when the nitrogen content in CO_2 BOG was varied from 5 mol% to 15 mol%.

3.3 Carbon Dioxide BOG Reliquefaction Process

Fig. 4 presents process flow diagrams of the CO_2 BOG reliquefaction processes considered in this study. In Cases 1, 2, and 3, the CO_2 BOG is first compressed to high pressure and then cooled to low temperatures through heat exchange with a refrigerant in a heat exchanger. Subsequently, it undergoes partial liquefaction by expanding to the tank pressure via a valve, and it is separated into gas and liquid phases in a vapor–liquid separator. The non-condensable gases are then vented to the atmosphere, and the liquefied CO_2 is returned to the tank.

For Cases 1 and 2, ammonia refrigerant applied widely in CO_2 liquefaction process studies was used as the refrigerant. Case 3 used a mixed refrigerant as the refrigerant, selecting ethane (C2), propane (C3), normal butane (nC4), and isobutane (iC4) as the components. The boiling point of pure CO_2 at 6.5 bar is −50.3 °C, and propane, with a boiling point of approximately −42.1 °C at atmospheric pressure, is sufficient to liquefy it. On the other hand, a lower cooling temperature may be necessary for liquefaction for mixtures containing substances

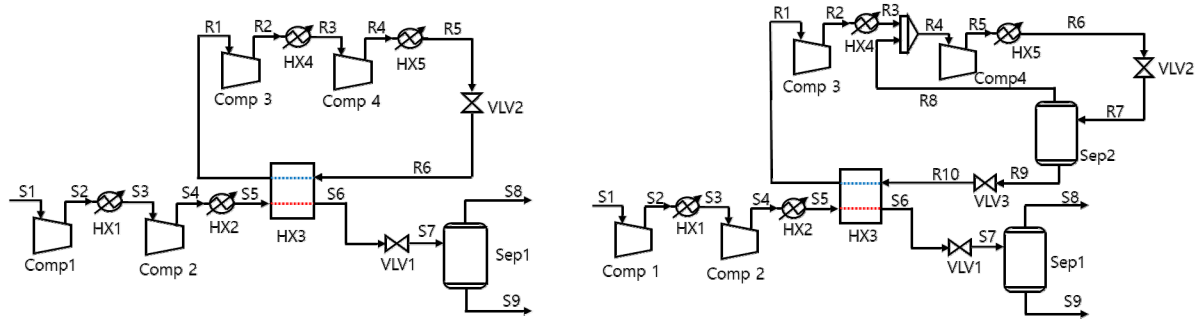

(a) Case 1 (b) Case 2

Fig. 4 CO_2 BOG reliquefaction process case 1–6 in this study

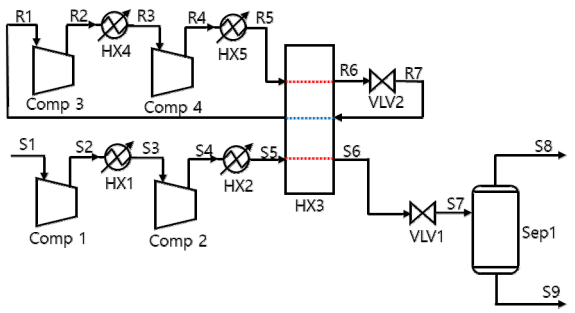

(c) Case 3

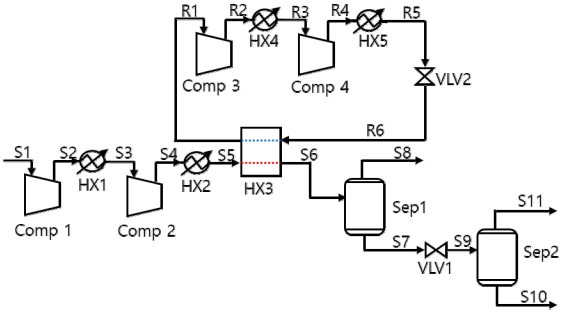

(d) Case 4

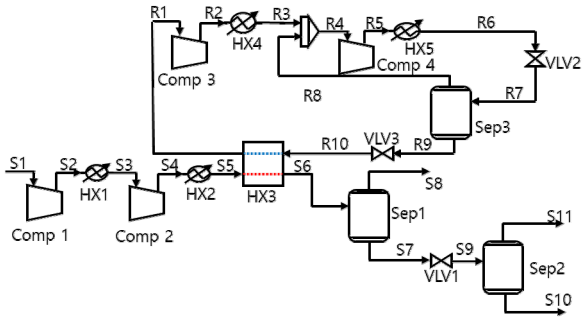

(e) Case 5

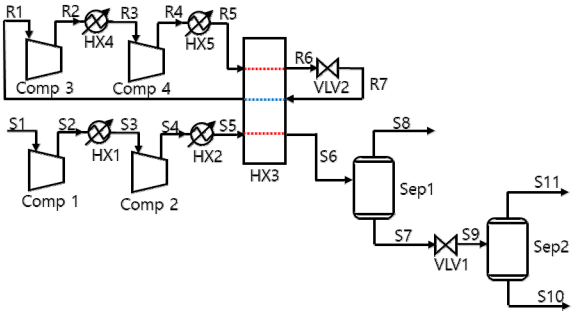

(f) Case 6

Fig. 4 CO_2 BOG reliquefaction process case 1–6 in this study (Continuation).

with lower boiling points, such as nitrogen. Therefore, ethane with a boiling point of approximately −88.5 °C at atmospheric pressure was included. Furthermore, normal butane and isobutane, with boiling points of approximately 0.5 °C and −11.7 °C, respectively, were included to improve the heat exchange efficiency in the high-temperature section of the heat exchanger.

Cases 4, 5, and 6 are process diagrams where an additional separator was installed in Cases 1, 2, and 3, respectively, to enhance the separation efficiency. Installing the additional separator serves to pre-release nitrogen, which vaporizes more readily than CO_2, sending high-purity CO_2 to the valve.

The Peng–Robinson equation of state was used to calculate the thermodynamic properties according to the pressure of liquid CO_2 (LCO_2). Each process was simulated using the commercial software Aspen HYSYS V11 under the conditions specified in Table 2 to ensure an equivalent comparison.

Table 2 Parameter and assumption for simulation

Items	Contents
Equation of state	Peng-Robinson
Refrigerant	Case 1, 2, 4, 5: ammonia Case 3, 6: mixed refrigerant (C2, C3, nC4, iC4)
Compressor adiabatic efficiency	75 %
Max. compressing ratio	3.0
Cooling water temp.	30 ℃
Cooler minimum temp. approach	5 ℃
Heat exchanger minimum temp. approach	3 ℃

3.4 Optimization Method for the Carbon Dioxide BOG Reliquefaction Process

Optimization was performed using the Particle Swarm Optimization (PSO) algorithm to find the optimal operating conditions for each

Table 3 Constraints and variables for optimization

Item	Var	Remark
Process constraints	Minimum temp approach ≥ 3.0 (°C)	HX3
	Pressure ratio ≤ 3.0	Comp1, 2, 3, 4
	Vapor fraction = 1.0	Comp1, 2, 3, 4 inlet
	Temperature ≥ −55.0 (°C)	S7 (Case 1, 2, 3) / S9 (Case 4, 5, 6)
Process variable	C2, C3, nC4, iC4 mass flow (t/h)	R1 (Case 3, 6)
	Pressure (bar)	R6 (Case 1, 4) / R2, R10 (Case 2, 5) / R5, R7 (Case 3, 6)
	Temperature (°C)	R1 (Case 1, 2, 4, 5) / R6 (Case 3, 6)
	Pressure ratio	Comp1, 2 (all case) / Comp3 (Case1, 3, 4, 6)

reliquefaction process and nitrogen content case. The Specific Power Consumption (SPC)—the energy consumption per unit production of liquefied CO_2— was set as the objective function to be minimized to achieve the optimal performance of the CO_2 reliquefaction process.

While satisfying the conditions in Table 2, optimization constraints were established to ensure that the temperature within the process remained above −55 °C even after the Joule–Thomson expansion of CO_2 to prevent liquid ingress and dry ice formation. If the constraints are violated, a penalty value is assigned to prevent the solution from being selected as the optimal value. The minimum SPC of the reliquefaction process was determined by considering key process variables, such as temperature, pressure, and refrigerant composition, as optimization variables for the reliquefaction process. These are summarized in Table 3.

4. Results

Among the optimization results of the reliquefaction systems, Table A1, A2 and Table 4 lists the cases where the nitrogen content in the CO_2 BOG was 5 mol% and 15 mol%. According to Table 4, when the nitrogen content in the CO_2 BOG was varied from 5–15 mol%, Cases 1, 2, and 3 showed a decrease in the total power consumption of the compressors as the compression ratio of the second compressor and the refrigerant flow rate decreased. In addition, the amount of reliquefied CO_2 decreased from 4,030, 4,080, and 4,296 kg/h at 5 mol% nitrogen to 570 kg/h at 15 mol% nitrogen. This is because the amount of cooling in the heat exchanger decreases, and the purge amount increases after Joule–Thomson expansion.

Fig. 5 shows the vapor fraction values of the stream after the Joule–Thomson expansion in each reliquefaction process. The vapor fraction after expansion increased as the nitrogen content in CO_2 increased, reaching up to 0.91 in Cases 1, 2, and 3. This was attributed to the minimum temperature constraint in the CO_2 reliquefaction process. If more nitrogen with a lower saturation temperature than CO_2 (−175.7 °C at 6.5 bar) is included, the phase equilibrium of the mixture shifts, resulting in the need for a lower temperature to produce the same amount of liquid under the same pressure conditions. In the BOG reliquefaction process, however, the lower temperature limit must be constrained to prevent dry ice formation. In this study, the formation of liquid after expansion was limited because the lower limit temperature

Table 4 Optimization result of (a) N_2 5 mol% and (b) N_2 15 mol%

(a) N_2 5 mol%

Item	Case 1	Case 2	Case 3	Case 4	Case 5	Case 6
Pressure ratio	PR_{Comp1}: 2.98 PR_{Comp2}: 1.50 PR_{Comp3}: 3.00	PR_{Comp1}: 3.00 PR_{Comp2}: 1.35	PR_{Comp1}: 3.00 PR_{Comp2}: 1.18 PR_{Comp3}: 3.00	PR_{Comp1}: 3.00 PR_{Comp2}: 1.32 PR_{Comp3}: 3.00	PR_{Comp1}: 3.00 PR_{Comp2}: 1.32	PR_{Comp1}: 3.00 PR_{Comp2}: 1.41 PR_{Comp3}: 3.00
Pressure(bar)	P_{R6}: 1.72	P_{R2}: 4.57 P_{R10}: 1.52	P_{R5}: 13.06 P_{R7}: 2.08	P_{R6}: 1.49	P_{R2}: 4.49 P_{R10}: 1.50	P_{R5}: 13.36 P_{R7}: 2.15
Temperature (°C)	T_{R1}: −21.84	T_{R1}: −24.51	T_{R6}: −26.62	T_{R1}: 32	T_{R1}: −23.07	T_{R6}: −28.31
Refrigerant mass flow (t/h)	$\dot{m}_{NH3}$: 1.62	$\dot{m}_{NH3}$: 1.44	$\dot{m}_{C2}$: 0.27 $\dot{m}_{C3}$: 4.35 $\dot{m}_{nC4}$: 0.81 $\dot{m}_{iC4}$: 0.07	$\dot{m}_{NH3}$: 1.50	$\dot{m}_{NH3}$: 1.43	$\dot{m}_{C2}$: 0.46 $\dot{m}_{C3}$: 3.55 $\dot{m}_{nC4}$: 1.02 $\dot{m}_{iC4}$: 0.81
W_{total}(kW)	352.8	344.0	347.6	357.4	342.7	374.1
$\dot{m}_{reliq}$(kg/h)	4030	4080	4296	4147	4135	4686
SPC (kWh/t)	87.5	84.3	80.9	86.2	82.9	79.8

(b) N_2 15 mol%

Pressure ratio	PR_{Comp1}: 2.98 PR_{Comp2}: 1.18 PR_{Comp3}: 3.00	PR_{Comp1}: 3.00 PR_{Comp2}: 1.18	PR_{Comp1}: 2.45 PR_{Comp2}: 1.01 PR_{Comp3}: 2.99	PR_{Comp1}: 3.00 PR_{Comp2}: 1.87 PR_{Comp3}: 3.00	PR_{Comp1}: 3.00 PR_{Comp2}: 1.86	PR_{Comp1}: 3.00 PR_{Comp2}: 1.18 PR_{Comp3}: 2.92
Pressure (bar)	P_{R6}: 1.49	P_{R2}: 4.47 P_{R10}: 1.49	P_{R5}: 11.95 P_{R7}: 1.35	P_{R6}: 1.49	P_{R2}: 4.47 P_{R10}: 1.49	P_{R5}: 16.71 P_{R7}: 2.06
Temperature (°C)	T_{R1}: 31.94	T_{R1}: −24.99	T_{R6}: −29.12	T_{R1}: 31.79	T_{R1}: −25.03	T_{R6}: −36.10
Refrigerant mass flow (t/h)	$\dot{m}_{NH3}$: 0.50	$\dot{m}_{NH3}$: 0.49	$\dot{m}_{C2}$: 0.01 $\dot{m}_{C3}$: 1.75 $\dot{m}_{nC4}$: 0.1 $\dot{m}_{iC4}$: 0.00	$\dot{m}_{NH3}$: 1.26	$\dot{m}_{NH3}$: 1.21	$\dot{m}_{C2}$: 0.72 $\dot{m}_{C3}$: 3.69 $\dot{m}_{nC4}$: 0.70 $\dot{m}_{iC4}$: 0.19
W_{total}(kW)	216.7	212.1	188.3	382.8	370.2	384.6
$\dot{m}_{reliq}$(kg/h)	570	570	570	3398	3389	4000
SPC (kWh/t)	380.0	372.0	330.2	112.6	109.3	96.2

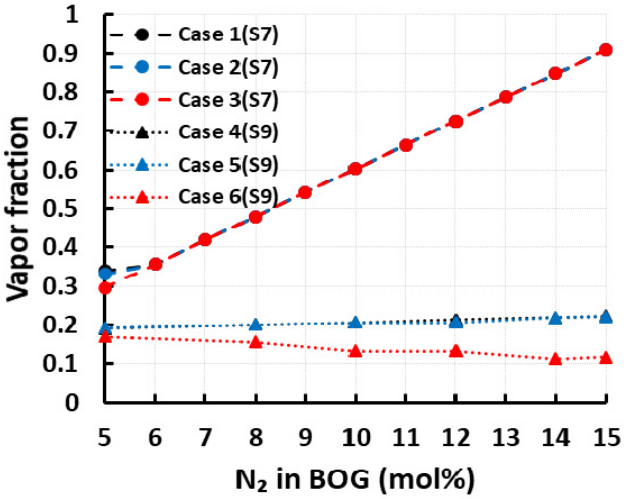

Fig. 5 Vapor fraction after JT (Joule–Thomson) expansion (Case 1–3: S7 Case 4–6: S9)

is restricted to −55 °C.

Therefore, in Cases 1, 2, and 3, as the nitrogen content increases, most of the CO_2 is purged due to the temperature constraint, resulting in decreases in the compression ratio of the second compressor, the refrigerant flow rate, and the amount of reliquefied CO_2. Consequently, in Cases 1, 2, and 3, when the nitrogen content varies from 5–15 mol%, the reliquefaction rate decreases from 69.4–74.0% to 10.6% (Fig. 6). Accordingly, although the total power consumption of the compressors decreased, the SPC increased exponentially from 87.5, 84.3, and 80.9 kWh/t to 380.0, 372.0, and 330.17 kWh/t, respectively (Fig. 6).

On the other hand, in Cases 4, 5, and 6, when the nitrogen content in the CO_2 BOG was varied from 5 mol% to 15 mol%, the SPC increased from 86.2, 82.9, and 79.8 kWh/t to 112.6, 109.3, and 96.2 kWh/t, respectively. On the other hand, the increase was relatively low, only approximately 20–30% (Fig. 6). This is because, in Cases 4, 5, and 6, the application of two-stage vapor–liquid separation keeps the vapor fraction after expansion low, at approximately 0.11–0.22, even though the total power consumption of the compressors increases to meet the lower saturation temperatures required as the nitrogen content rises (Fig. 5). This allows for an increased amount of reliquefied CO_2 compared to Cases 1, 2, and 3.

By applying two-stage vapor–liquid separation, lighter nitrogen gas can be separated from CO_2 before expansion, allowing for Joule–Thomson expansion of CO_2 with relatively higher purity. This makes it possible to increase the amount of reliquefied CO_2 even at the limited temperature of −55 °C compared to Cases 1, 2, and 3. Consequently, a reliquefaction rate of over 63.0% was achieved in Cases 4 and 5, even when the nitrogen content was increased to 15 mol%. In Case 6, which uses mixed refrigerants, a reliquefaction rate of 74.2% can be achieved under the same conditions.

Reliquefaction is possible when using mixed refrigerants because of the more efficient heat exchange. Fig. 7 shows the thermal composite curves of Cases 4 and 6 when the nitrogen content is 15 mol%. The temperature difference between the hot and cold composite curves is, on average, 18 °C with a maximum of 38.5 °C in Case 4, whereas in Case 6, it is, on average, 11 °C with a maximum of 32. 2 °C. This suggests that more efficient heat exchange is occurring in Case 6 using mixed refrigerants. This efficiency is achieved because mixed refrigerants composed of substances with different boiling points can utilize the latent heat of each refrigerant in the BOG reliquefaction process.

As a result, the proposed two-stage vapor–liquid separation process increased the amount of liquefied CO_2 compared to the single vapor–liquid separation process. When the nitrogen content changed from 5 mol% to 15 mol%, the reliquefaction rate of Case 1, which uses ammonia refrigerant in a single vapor–liquid separation process, decreased sharply from 69.4% to 10.6%. In contrast, Case 6, which applies mixed refrigerants and a two-stage vapor–liquid separation process, achieved a reliquefaction rate of over 74.2% in all cases.

Maintaining the reliquefaction rate also led to significant variations

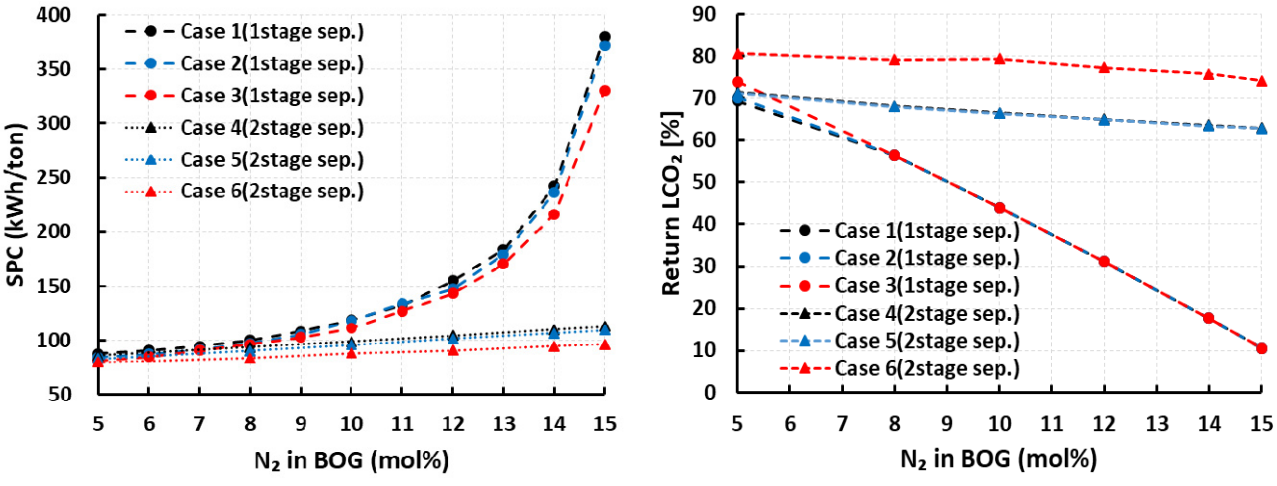

(a) (b)

Fig. 6 Optimization result of (a) SPC and (b) Return LCO_2 fraction

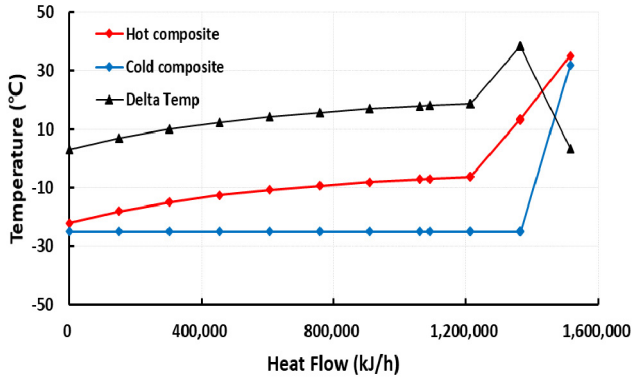

(a)

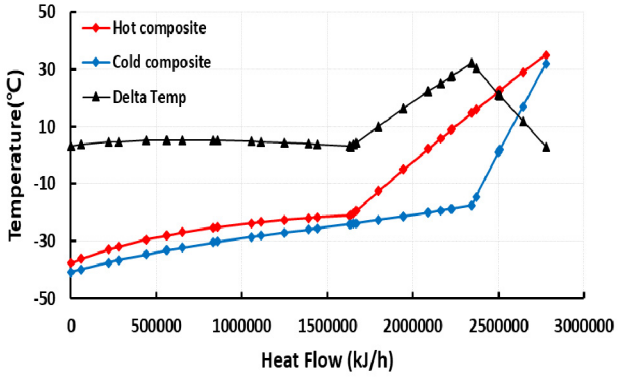

(b)

Fig. 7 Heat curve of (a): Case 4 and (b): Case 6 at N_2 15 mol%

in the energy consumption required for the liquefaction process. When the nitrogen content was 5 mol%, the SPC of Case 1 was 87.5 kWh/t, whereas the SPC was 79.8 kWh/t in Case 6, showing an 8.8% reduction in SPC. As the nitrogen content increased, the effect of the two-stage separation process became more pronounced. When the nitrogen content was 15 mol%, the SPC of Case 6 was 96.2 kWh/t, showing a 74.7% reduction compared to the SPC of 380.0 kWh/t in Case 1.

5. Conclusion

Optimization was performed to minimize the specific power consumption (SPC) for cases where the nitrogen content in CO_2 BOG varies from 5.0 to 15.0 mol%, considering the use of ammonia as a refrigerant (Cases 1 and 2) and the use of mixed refrigerants (Case 3). In the reliquefaction processes applying single-stage vapor–liquid separation (Cases 1, 2, and 3), the amount of reliquefied CO_2 decreased sharply as the impurity content increased, leading to a significant drop in efficiency. This is because higher amounts of nitrogen, which has a lower saturation temperature, shift the phase equilibrium, requiring lower temperatures for reliquefaction. On the other hand, a temperature limit of −55 °C was imposed to avoid the possibility of dry ice formation, restricting liquid formation.

Therefore, cases were also optimized and compared by applying a two-stage vapor–liquid separation process (Cases 4, 5, and 6) to address the issue of decreasing reliquefaction rates with increasing nitrogen content. In the reliquefaction processes with an additional vapor–liquid separator before expansion (Cases 4, 5, and 6), efficient reliquefaction was possible because lighter nitrogen was removed before the Joule–Thomson expansion compared to CO_2. As a result, the processes with an added vapor–liquid separator (Cases 4, 5, and 6) could achieve an SPC reduction of 1.6–74.7% compared to Cases 1, 2, and 3.

Among these, Case 6 allowed for efficient heat exchange using mixed refrigerants, making it possible to expect an additional SPC reduction of 7.4–14.6% compared to Cases 4 and 5. Consequently, in the process of applying the vapor–liquid separator and mixed refrigerants (Case 6), an SPC reduction of 8.8–74.7% could be expected compared to the existing process design. Only Case 6 showed a reliquefaction rate of over 74.2% across all nitrogen content ranges from 5% to 15%.

When impurities, such as nitrogen, increased in the CO_2 BOG, the reliquefaction rate decreased gradually, and the amount of non-condensable gas vented to the atmosphere increased. This leads to increased greenhouse gas emissions and causes economic losses due to cargo loss from the perspective of CO_2 carriers. Therefore, future studies will be needed to design reliquefaction processes considering economic aspects during CO_2 transportation.

Conflict of Interest

Youngsub Lim serves as an editorial board member of the Journal of Ocean Engineering and Technology but played no role in deciding the publication of this article. No potential conflicts of interest relevant to this study are reported.

Funding

This research was supported by Korea Institute of Marine Science & Technology Promotion(KIMST) funded by the Ministry of Oceans and Fisheries(2520000243), and the Korea Research Institute of Ships and Ocean engineering, grant from Endowment Project of “Technology Development of Onboard Carbon Capture and Storage System and Pilot Test” funded by Ministry of Oceans and Fisheries (PES5110). The Research Institute of Marine Systems Engineering and Institute of Engineering Research at Seoul National University provided research facilities.

References

Alabdulkarem, A., Hwang, Y., & Radermacher, R. (2012). Development of CO_2 liquefaction cycles for CO_2 sequestration. Applied Thermal Engineering, 33–34, 144–156. https://doi.org/10.1016/j.applthermaleng.2011.09.027

Aliyon, K., Mehrpooya, M., & Hajinezhad, A. (2020). Comparison of different CO2 liquefaction processes and exergoeconomic evaluation of integrated CO2 liquefaction and absorption refrigeration system. Energy Conversion and Management, 211, 112752. https://doi.org/https://doi.org/10.1016/j.enconman.2020.112752

Chen, F., & Morosuk, T. (2021). Exergetic and economic evaluation of CO_2 liquefaction processes. Energies, 14(21), 7174. https://www.mdpi.com/1996-1073/14/21/7174

Chu, B., Chang, D., & Chung, H. (2012). Optimum liquefaction fraction for boil-off gas reliquefaction system of semi-pressurized liquid CO_2 carriers based on economic evaluation. International Journal of Greenhouse Gas Control, 10, 46−55. https://doi.org/10.1016/j.ijggc.2012.05.016

Decarre, S., Berthiaud, J., Butin, N., & Guillaume-Combecave, J.-L. (2010). CO_2 maritime transportation. International Journal of Greenhouse Gas Control, 4(5), 857−864. https://doi.org/10.1016/j.ijggc.2010.05.005

Deng, H., Roussanaly, S., & Skaugen, G. (2019). Techno-economic analyses of CO_2 liquefaction: Impact of product pressure and impurities. International Journal of Refrigeration, 103, 301−315. https://doi.org/https://doi.org/10.1016/j.ijrefrig.2019.04.011

IRENA. (2022), Global Hydrogen Trade to Meet the 1.5 °C Climate Goal. Vol. Part 1.

Jackson, S., & Brodal, E. (2019). Optimization of the CO_2 Liquefaction Process-Performance Study with Varying Ambient Temperature. Applied Sciences, 9(20), 4467. https://www.mdpi.com/2076-3417/9/20/4467

Jeon, S. H., & Kim, M. S. (2015). Effects of impurities on reliquefaction system of liquefied CO_2 transport ship for CCS. International Journal of Greenhouse Gas Control, 43, 225−232. https://doi.org/10.1016/j.ijggc.2015.10.011

Kennedy, J., & Eberhart, R. (1995, November 27−December 1). Particle swarm optimization. In *Proceedings of ICNN'95 - International Conference on Neural Networks* (Vol. 4, pp. 1942−1948). IEEE. https://doi.org/1109/ICNN.1995.488968

Khan, M. S., & Lee, M. (2013). Design optimization of single mixed refrigerant natural gas liquefaction process using the particle swarm paradigm with nonlinear constraints. *Energy, 49*, 146−155. https://doi.org/10.1016/j.energy.2012.11.028

Lee, J., Son, H., Oh, J., Yu, T., Kim, H., & Lim, Y. (2024). Advanced process design of subcooling reliquefaction system considering storage pressure for a liquefied CO_2 carrier. *Energy, 293*, 130556. https://doi.org/https://doi.org/10.1016/j.energy.2024.130556

Lee, J., Son, H., Yu, T., Oh, J., Park, M. G., & Lim, Y. (2023). Process design of advanced LNG subcooling system combined with a mixed refrigerant cycle. Energy, 278(Part A), 127892. https://doi.org/https://doi.org/10.1016/j.energy.2023.127892

Lee, S. G., Choi, G. B., Lee, C. J., & Lee, J. M. (2017a). Optimal design and operating condition of boil-off CO_2 reliquefaction process, considering seawater temperature variation and compressor discharge temperature limit. Chemical Engineering Research and Design, 124, 29−45. https://doi.org/10.1016/j.cherd.2017.05.029

Lee, S. G., Choi, G. B., & Lee, J. M. (2015). Optimal design and operating conditions of the CO_2 liquefaction process, considering variations in cooling water temperature. Industrial & Engineering Chemistry Research, 54(51), 12855−12866. https://doi.org/10.1021/acs.iecr.5b02391

Lee, Y., Baek, K. H., Lee, S., Cha, K., & Han, C. (2017b). Design of boil-off CO2 reliquefaction processes for a large-scale liquid CO_2 transport ship. International Journal of Greenhouse Gas Control, 67, 93−102. https://doi.org/10.1016/j.ijggc.2017.10.008

Lu, J., Li, Y., Li, B., Yang, Q., & Deng, F. (2023). Research on reliquefaction of cargo BOG using liquid ammonia cold energy on CO_2 transport ship. International Journal of Greenhouse Gas Control, 129, 103994. https://doi.org/10.1016/j.ijggc.2023.103994

Moein, P., Sarmad, M., Ebrahimi, H., Zare, M., Pakseresht, S., & Vakili, S. Z. (2015). APCI- LNG single mixed refrigerant process for natural gas liquefaction cycle: Analysis and optimization. Journal of Natural Gas Science and Engineering, 26, 470−479. https://doi.org/10.1016/j.jngse.2015.06.040

Seo, Y., You, H., Lee, S., Huh, C., & Chang, D. (2015). Evaluation of CO2 liquefaction processes for ship-based carbon capture and storage (CCS) in terms of life cycle cost (LCC) considering availability. International Journal of Greenhouse Gas Control, 35, 1−12. https://doi.org/10.1016/j.ijggc.2015.01.006

Seo, Y., Huh, C., Lee, S., & Chang, D. (2016). Comparison of CO_2 liquefaction pressures for ship-based carbon capture and storage (CCS) chain. International Journal of Greenhouse Gas Control, 52, 1−12. https://doi.org/10.1016/j.ijggc.2016.06.011

Tsivintzelis, I., & Kontogeorgis, G. M. (2015). Modelling phase equilibria for acid gas mixtures using the CPA equation of state. Part V: Multicomponent mixtures containing CO_2 and alcohols. The Journal of Supercritical Flluids, 104, 29−39. https://doi.org/10.1016/j.supflu.2015.05.015

Xu, X., Liu, J., Jiang, C., & Cao, L. (2013). The correlation between mixed refrigerant composition and ambient conditions in the PRICO LNG process. Applied Energy, 102, 1127−1136. https://doi.org/10.1016/j.apenergy.2012.06.031

Yoo, B.-Y. (2017). The development and comparison of CO_2 BOG reliquefaction processes for LNG fueled CO_2 carriers. Energy, 127, 186−197. https://doi.org/10.1016/j.energy.2017.03.073

Zhang, J., Meerman, H., Benders, R., Faaij, A., (2020). Comprehensive reviewof current natural gas liquefaction processes on technical and economic performance. Applied Thermal Engineering, 166, 114736. https://doi.org/10.1016/j.applthermaleng.2019.114736

Author ORCIDs

Author name	ORCID
Jeong, Ijun	0009-0006-7979-6989
Lim, Youngsub	0000-0001-9228-0756

Appendices

Table A1 Simulation result of N_2 5 mol%

Case	Stream	Pressure (bar)	Temperature (℃)	Mass flow (t/h)
Case 1	S1	6.5	-28.5	6.0
	S5	29.0	35.0	6.0
	S6	29.0	-18.9	6.0
	S7	6.5	-54.4	6.0
	S9 (product)	6.5	-54.4	4.0
	R1	1.7	-21.8	1.6
	R5	13.4	35.0	1.6
	R6	1.7	-21.8	1.6
Case 2	S1	6.5	-28.5	6.0
	S5	26.3	35.0	6.0
	S6	26.3	-21.6	6.0
	S7	6.5	-54.5	6.0
	S9 (product)	6.5	-54.5	4.1
	R1	1.5	-24.5	1.4
	R6	13.4	35.0	1.7
	R10	1.5	-24.5	1.4
Case 3	S1	6.5	-28.5	6.0
	S5	23.0	35.0	6.0
	S6	23.0	-26.6	6.0
	S7	6.5	-55.0	6.0
	S9 (product)	6.5	-55.0	4.3
	R1	2.1	32.0	5.5
	R5	13.1	35.0	5.5
	R6	13.1	-26.6	5.5
	R7	2.1	-29.6	5.5
Case 4	S1	6.5	-28.5	6.0
	S5	25.7	35.0	6.0
	S6	25.7	-22.0	6.0
	S9	6.5	-52.2	6.0
	S10 (product)	6.5	-52.2	4.1
	R1	1.5	32.0	1.5
	R5	13.4	35.0	1.5
	R6	1.5	-25.0	1.5
Case 5	S1	6.5	-28.5	6.0
	S5	25.7	35.0	6.0
	S6	25.7	-21.9	6.0
	S9	6.5	-52.2	6.0
	S10 (product)	6.5	-52.2	4.1
	R1	1.5	-23.1	1.4
	R6	13.4	35	1.6
	R10	1.5	-24.9	1.4
Case 6	S1	6.5	-28.5	6.0
	S5	27.4	35.0	6.0
	S6	27.4	-28.3	6.0
	S9	6.5	-53.8	6.0
	S10 (product)	6.5	-53.8	4.7
	R1	2.1	32.0	5.8
	R5	13.4	35.0	5.8
	R6	13.4	-28.3	5.8
	R7	2.2	-31.3	5.8

Table A2 Simulation result of N_2 15 mol%

Case	Stream	Pressure (bar)	Temperature (℃)	Mass flow (t/h)
Case 1	S1	6.5	-28.5	6.0
	S5	22.9	35.0	6.0
	S6	22.9	-22.0	6.0
	S7	6.5	-55.0	6.0
	S9 (product)	6.5	-55.0	0.6
	R1	1.5	32.0	0.5
	R5	13.4	35.0	0.5
	R6	1.5	-25.0	0.5
Case 2	S1	6.5	-28.5	6.0
	S5	22.9	35.0	6.0
	S6	22.9	-22.0	6.0
	S7	6.5	-55.0	6.0
	S9 (product)	6.5	-55.0	0.6
	R1	1.5	-25.0	0.5
	R6	13.4	35.0	0.6
	R10	1.5	-25.0	0.6
Case 3	S1	6.5	-28.5	6.0
	S5	16.1	35.0	6.0
	S6	16.1	-32.2	6.0
	S7	6.5	-55.0	6.0
	S9 (product)	6.5	-55.0	0.6
	R1	1.3	32.0	1.9
	R5	12.0	35.0	1.9
	R6	12.0	-29.1	1.9
	R7	1.3	-35.2	1.9
Case 4	S1	6.5	-28.5	6.0
	S5	36.5	35.0	6.0
	S6	36.5	-22.0	6.0
	S9	6.5	-54.3	6.0
	S10 (product)	6.5	-54.3	3.4
	R1	1.5	31.8	1.3
	R5	13.4	35.0	1.3
	R6	1.5	-25.0	1.3
Case 5	S1	6.5	-28.5	6.0
	S5	36.3	35.0	6.0
	S6	36.3	-22.0	6.0
	S9	6.5	-54.3	6.0
	S10 (product)	6.5	-54.3	3.4
	R1	1.5	-25.0	1.2
	R6	13.4	35.0	1.4
	R10	1.5	-25.0	1.2
Case 6	S1	6.5	-28.5	6.0
	S5	23.0	35.0	6.0
	S6	23.0	-37.7	6.0
	S9	6.5	-55.0	6.0
	S10 (product)	6.5	-55.0	4.0
	R1	2.1	32.0	5.3
	R5	16.7	35.0	5.3
	R6	16.7	-36.1	5.3
	R7	2.1	-40.7	5.3